Lattice Boltzmann Simulation of Transonic Rotor Aerodynamics and Acoustics

Naina Pisharoti
SIMULIA Fluids R&D
Dassault Systèmes Americas Corp.
Waltham, MA, USA

Gianluca Romani
SIMULIA Fluids R&D
Dassault Systèmes Deutschland GmbH
Stuttgart, Germany

Damiano Casalino
SIMULIA Fluids R&D
Dassault Systèmes Deutschland GmbH
Stuttgart, Germany

ABSTRACT

This paper presents the validation and assessment of rotorcraft High-Speed Impulsive (HSI) noise prediction using a high-fidelity Lattice Boltzmann / Very Large Eddy Simulation (LB/VLES) transonic solver, SIMULIA PowerFLOW®, coupled with the time-domain Ffowcs–Williams Hawkings (FW-H) solver, SIMULIA PowerACOUSTICS®. A benchmark transonic rotor case featuring high-subsonic and transonic tip speeds is used for the analysis. Flow predictions reveal the formation of localized supersonic pockets on the blade surface and the development of a shock spiral in the rotor plane. As the tip speed increases, the solver accurately captures the associated shock de-localization characteristic of transonic rotors. The resulting HSI noise—driven by these shock dynamics—is well predicted by the computational framework, demonstrating good agreement with experimental data.

INTRODUCTION

Modeling the flow around helicopter rotors presents significant challenges due to the inherently complex, unsteady, and highly non-linear nature of the flow field. The high tip speeds at which these rotors typically operate — often within the transonic regime — lead to the formation of shocks. When the tip Mach number exceeds a certain critical value ($M \geq 0.8$), localized supersonic flow pockets form, creating nonlinear shock regions at the rotor tip. As the tip speed further increases, the shock region expands, leading to the formation of de-localized shock regions and the generation of the so-called High-Speed Impulseve (HSI) noise. In forward flight, the impulsive character of this phenomenon is magnified by the periodic modulation of the transonic region. Due to physical complexity of these aerodynamic and aeroacoustic mechanisms, the accurate numerical simulation of rotors in transonic regimes remains a significant challenge for CFD software.

Over the past few decades, considerable efforts have been devoted to the numerical prediction of High Speed Impulsive (HSI) noise in transonic rotor environments. Most studies employ an acoustic analogy framework, in which the aerodynamic field is first computed using a CFD solver, and the resulting acoustic field is then obtained through an integral formulation for noise propagation. For this purpose, the permeable Ffowcs Williams–Hawkings (FW-H) formulation is widely used (Ref. 1). However, a well-known limitation of the FW-H approach is the emergence of a Doppler singularity in the integral kernel when the relative Mach number approaches unity ($M_r = 1$), along with additional complexities at transonic and supersonic speeds. To overcome these challenges, researchers have proposed various mitigation strategies, such as emission surface algorithms (Refs. 2–5) and advanced-time integration techniques (Refs. 6, 7).

In modeling the rotor flow, Euler-based solvers are frequently employed, since HSI noise is predominantly influenced by inviscid shock-related phenomena (Refs. 2, 4, 8–10). Among these efforts, D'Alascio et al. (Ref. 10) demonstrated the capability of an unsteady Euler solver, EROS, coupled with the acoustic solver HERNOP3, to predict HSI noise for tip Mach numbers ranging from 0.85 to 0.95. At higher Mach numbers ($M > 0.9$), however, they reported an over-prediction of the negative acoustic pressure peak, attributed to the acoustic solver's inability to account for supersonic source mechanisms. More recently, Fu and Vigevano (Ref. 5) employed a RANS-based CFD solver in combination with a permeable FW-H formulation enhanced by a marching cube emission surface algorithm (Ref. 3), and validated their framework against two benchmark transonic rotor geometries, demonstrating good agreement with experimental data.

In recent years, the lattice-Boltzmann method (LBM) has been developed as an alternative CFD method for numerical simulations of unsteady turbulent flows. Unlike traditional Navier–Stokes methods, which model fluids at the continuum level, the LBM operates at a mesoscopic scale using discrete particle distribution functions, from which macroscopic flow properties emerge through moment operations. Its explicit and local formulation allows for efficient parallelization and facilitates the modeling of complex fluids, geometries, and boundary conditions (Refs. 11–13). Additionally, LBM's low dissipation, inherent compressibility, and unsteady solution capability make it particularly well suited for aeroacoustic simulations. As a result, LBM has evolved into a robust and mature CFD methodology for large-scale simulations of complex industrial aeroacoustic applications, including airframe (Refs. 14–16), propeller (Refs. 17, 18), and helicopter blade–vortex interaction noise (Refs. 19, 20), as well as turbofan engine (Refs. 21, 22) and jet installation noise (Ref. 23).

Until recently, the use of multi-layer lattice models within the Lattice Boltzmann Method (LBM) for high-speed transonic flows was limited by excessive numerical dissipation and high computational cost. To overcome these challenges, Li et al. (Ref. 24) presented a hybrid solver that combines a multi-layer lattice model—suitable for transonic regimes—with a single-layer lattice model traditionally used for weakly compressible subsonic flows. In this framework, the multi-layer model is applied in transonic regions, while the single-layer model handles high-speed subsonic areas. This hybrid approach broadens the solver's applicability across a wider range of Mach numbers while preserving the low numerical dissipation characteristic of the subsonic model. As a result, it has opened the door to more accurate modeling of flow around transonic rotors.

The primary objective of the present study is to demonstrate the capability of the high-fidelity Lattice Boltzmann / Very Large Eddy Simulation (LB/VLES) solver, SIMULIA PowerFLOW®, in predicting rotorcraft High-Speed Impulsive (HSI) noise. While an earlier version of the solver was successfully applied to the prediction of blade–vortex interaction noise for an elastic rotor in descending flight (Refs. 19, 20), the present work focuses on capturing the nonlinear flow mechanisms responsible for HSI noise generation at tip Mach numbers approaching supersonic speeds, using the newly integrated hybrid solver discussed previously. Although HSI noise is primarily an inviscid phenomenon, this study aims to validate the solver's effectiveness in capturing this fundamental yet complex mechanism. This effort represents an important step toward enabling accurate full-rotorcraft simulations under transonic operating conditions.

NUMERICAL METHOD

LB/VLES Flow Solver

The commercial CFD/CAA solver SIMULIA PowerFLOW®, based on the lattice-Boltzmann method, is used in the present work to simulate the flow field around the transonic rotor. The lattice-Boltzmann approach is based on a mesoscopic description of the fluid, where collections of particles are tracked through the so-called particle distribution function $f(\mathbf{x},\mathbf{c},t)$, representing the density of particles with microscopic velocity $\mathbf{c}$ at position $\mathbf{x}$ and time t. The evolution in time of $f(\mathbf{x},\mathbf{c},t)$ is governed by the Boltzmann equation, which is discretized in the physical space and time, as well as in the microscopic velocity domain into a prescribed set of velocity directions $\mathbf{c}_i$. In PowerFLOW®, a regularized discrete lattice-Boltzmann equation with the filtered collision operator satisfying Galilean invariance (Ref. 25), is employed:

$$f_i(\mathbf{x}+\mathbf{c}_i\delta t, t+\delta t) = f_i^{\mathrm{eq}}(\mathbf{x},t) + \left(1-\frac{1}{\tau}\right)\hat{f}_i^{\mathrm{neq}}(\mathbf{x},t), \quad (1)$$

where f_i is the particle distribution function along the i-th lattice direction, δt is the discrete time increment, τ is the single relaxation time parameter, while f_i^{eq} and $\hat{f}_i^{\mathrm{neq}}$ are the equilibrium and filtered non-equilibrium discrete distributions, respectively. Finally, The macroscopic flow variables are derived by taking appropriate moments of the distribution functions.

The LBM scheme is implemented on a Cartesian mesh composed of cubic volume elements (voxels) arranged across multiple Variable Resolution (VR) regions. A resolution change by a factor of two is allowed between adjacent VRs. Since the solver uses an explicit time-marching scheme with a unit Courant–Friedrichs–Lewy (CFL) condition, the time step, based on the lattice spacing and velocity, also changes by a factor of two between adjacent VRs. Solid surfaces are discretized within each voxel intersecting the geometry using planar surface elements (surfels). No-slip and slip wall boundary conditions are applied via a bounce-back and specular reflection scheme, respectively (Ref. 11). This allows for rapid and automated meshing of complex geometries, avoiding the manual effort required by body-fitted meshing in traditional CFD methods.

In this study, a hybrid subsonic/transonic solver is employed to simulate the flow around the rotor, with a separate macroscopic equation for total energy solved by a lattice-Boltzmann algorithm satisfying the exact energy conservation (Refs. 26, 27). To simulate rotating geometries, the computational domain is partitioned into an outer inertial reference frame and a Local Reference Frame (LRF). The LRF is implemented as a volume-based sliding mesh that undergoes rigid-body rotation with the rotating geometry, thereby eliminating relative motion between the mesh and the enclosed solid surface. Within this rotating frame, Eq. (1) is solved with an additional body force term, which accounts for inertial effects associated with the non-inertial reference frame (Ref. 28). In the rotating domain, a multi-layer transonic LBM scheme is used, whereas outside the LRF, a single-layer subsonic LBM scheme is used.

While LBM is capable of performing Direct Numerical Simulation (DNS), the computational cost is typically prohibitive for industrial applications, making turbulence modeling necessary. In PowerFLOW®, the LBM scheme is coupled with a modified two-equation RNG k–ε model (Refs. 29–31) to compute a turbulent relaxation time, which is incorporated into the effective relaxation process governing particle collisions.

Due to the Cartesian grid, anisotropic cell stretching near walls (e.g., only in the wall-normal direction) is not possible. As a result, resolving boundary layers down to the wall with fine near-wall spacing is often too computationally expensive. To mitigate this, a wall function approach is employed, extending the standard law-of-the-wall formulation (Ref. 32) and incorporating pressure gradient effects (Ref. 33), allowing for efficient modeling of near-wall flows.

Far-field Noise Solver

The LBM is inherently transient and compressible, and would allow to directly extract the acoustic field from the flow solution. However, to reduce computational cost, a coupled CFD/CAA approach is employed to more efficiently compute far-field noise, avoiding the high computational cost of directly resolving acoustic wave propagation to the far field. To this end, a permeable Ffowcs Williams–Hawkings (FW-H) acoustic analogy (Ref. 34) is applied, using flow variables from the LBM solution extracted on a non-rotating permeable integration surface that encloses the primary noise sources. The FW-H solver used is part of the SIMULIA PowerACOUSTICS® post-processing suite and is based on a forward-time implementation (Ref. 35) of Farassat's Formulation 1A (Ref. 36). This formulation neglects the volume (quadrupole) integral, which would otherwise capture nonlinear effects, such as shock waves, turbulence mixing, and nonlinear propagation in the volume region outside the control surface. However, by ensuring that the integration surface fully encloses all relevant quadrupole noise sources, these contributions can still be recovered through the surface integral terms.

TEST CASE AND COMPUTATIONAL SETUP

Benchmark Case

Purcell (Ref. 37) conducted an experimental campaign in the NASA anechoic chamber to capture HSI noise by designing a test setup using a scale model of the UH-1H main rotor in hover. The experiment measured the noise generated by the isolated rotor at different tip Mach numbers ranging from $M_T = 0.85$ to $M_T = 0.95$. Although HSI noise typically occurs in forward flight, the test was conducted in hover, as the high tip speeds replicated conditions on the advancing blade. The rotor has an untwisted blade geometry with a NACA0012 airfoil section. It has a radius of $R = 1.044$ m and a constant chord length of $c = 0.0762$ m. The simple geometry allows for easy reproducibility, facilitating validation against the experimental database. This makes it an excellent candidate for the current study.

In this paper, two operating conditions with tip Mach numbers of $M_T = 0.85$ and 0.95 are considered. The rotor is known to exhibit a localized shock at $M_T = 0.85$, whereas at $M_T = 0.95$, the shock becomes de-localized (Refs. 4, 37). This makes the highest tip Mach number case a particularly challenging case to simulate and of specific interest in this study. Figure 1 shows the blade geometry along with the mic position that aligns with the experiment.

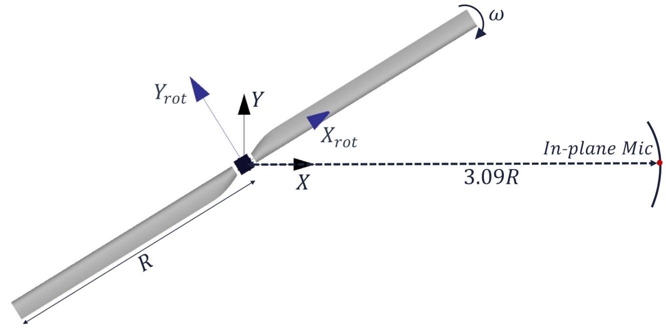

Figure 1. UH-1H Rotor Geometry and Mic Set-up (top-view)

Computational Setup

The computational fluid domain is a large spherical volume of radius $\approx 400R$, centered around the propeller hub. The computational domain and resolution surrounding the rotor is shown in 2. A total of 16 variable resolution (VR) levels were used for the set-up, with VR15 being the finest and set to discretize the region closest to the blade wall. The voxel (grid cell) size between each successive VR region increases by a factor of two. The rotor is surrounded by a volume of revolution called the Local Reference Frame (LRF) region (as also shown in Figure 3), namely the rotating sliding mesh domain used to reproduce the propeller rotation. It is placed at an offset of 0.09 m from the rotor tip and given a refinement level of VR12. The helicopter rotor was simulated using a hybrid solver, where the region inside the Local Refinement Field (LRF) was solved using the multi-layer lattice model to capture transonic effects, while the region outside the LRF employed the single-layer lattice model, as it lies predominantly in the high-subsonic regime.

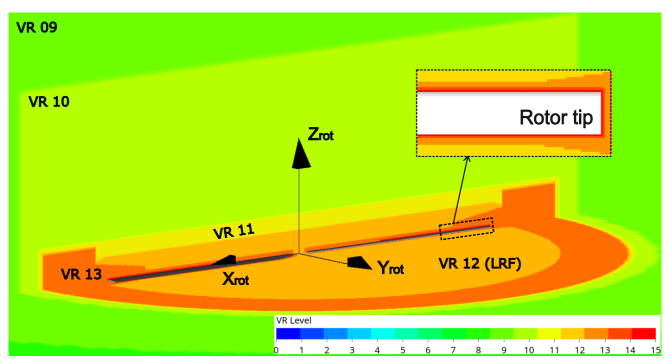

Figure 2. Near-body computational grid

The noise generated by the rotor is computed using the time-domain FWH tool SIMULIA PowerACOUSTICS®, which employs a permeable integration surface for the calculation. The permeable FW-H surface is placed outside the LRF at an offset of 0.2 m from the rotor tip, as shown in Figure 3. This offset was chosen to capture most of the quadrupole sources within the permeable surface. The region outisde the LRF and within the FWH is refined to a finer resolution of VR13 (within the dark orange region shown in fig. 2), to ensure that

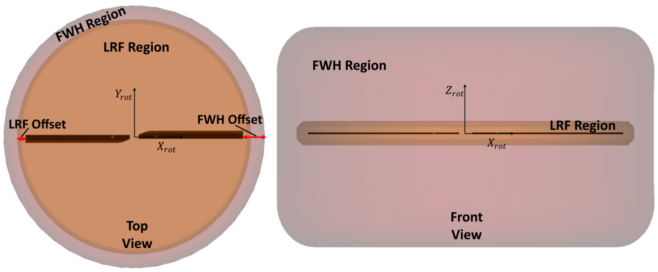

Figure 3. Depiction of the LRF and FWH regions in the computational domain

the shock spiral is captured accurately. For the aeroacoustic calculations, the flow data is sampled over 5 rotor revolutions, following an initial run of two revolutions to ensure convergence. All the acoustic results included in this work are phase-averaged pressure signals.

Resolution Study

A resolution study was carried out to assess the influence of the grid on the flow and acoustic predictions. The case with $M_{tip} = 0.95$ was chosen. Each computational grid was successively increased by a factor of $\sqrt{2}$ globally.

Figure 4 presents the surface pressure distribution at various spanwise locations along the rotor blade. The pressure has been non-dimensionalized using the dynamic pressure with respect to the span-wise location. At the 70% span position, the results show no noticeable sensitivity to the grid resolution. In contrast, the outer sections—where the pressure distribution is influenced by shock waves exhibit some grid sensitivity, particularly near the shock location, indicated by the abrupt drop in C_p. Figure 5 shows the acoustic pressure pulse, where both the “Medium” and “Fine” grids accurately capture the positive and negative pressure peaks, in contrast to the “Coarse” grid. Based on this, the ”Fine” grid is selected for the subsequent analysis.

NUMERICAL RESULTS

The surface pressure predictions for $M_{tip} = 0.85$ and 0.95 are shown in Figures 6 & 7 respectively. As M_{tip} increases, the shock wave occurs earlier along the span. Figure 8 shows the Mach contour over and around the blade. The contour slice shown here was placed at an offset of 5 mm below the rotor plane to visualize the contours on the blade as well. For the lowest tip Mach number, the supersonic region is confined to the blade surface, close to the tip and hence, localized. On the other hand, at the higher Mach number, the shock delocalization is visible, wherein the shock bleeds out of the blade and tends to merge into the sonic circle (indicated by the yellow contour region beyond the tip). Further, the supersonic pocket on the blade surface is much larger for $M_{tip} = 0.95$ case. Figure 9 shows the static pressure contour along the rotor plane over a slice which stretches up to ≈ 2.3 times the radius of the rotor. The contour displays a distinct spiral in all cases, caused by the occurrence of the shock. As expected,

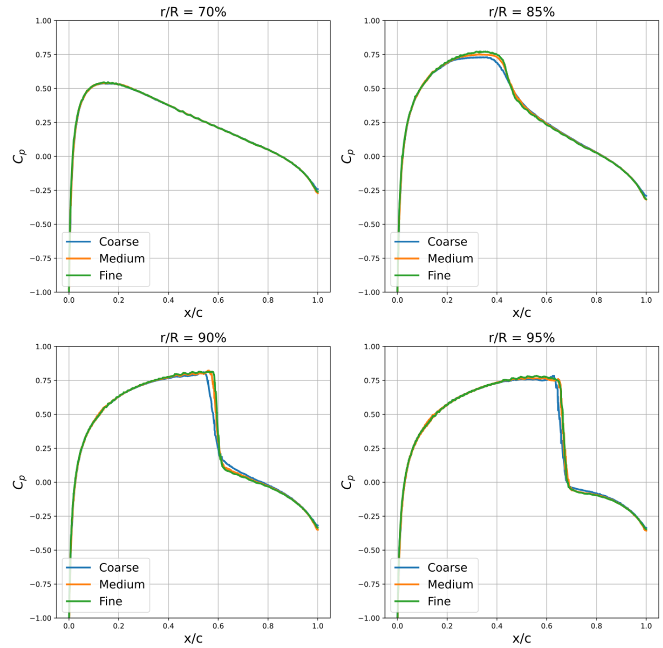

Figure 4. Grid sensitivity demonstrated using the surface pressure distribution at different span-wise locations for $M_{tip} = 0.95$

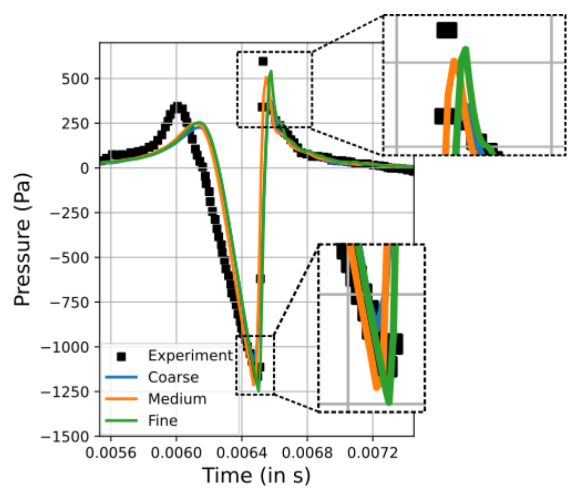

Figure 5. Grid sensitivity demonstrated using the acoustic pressure pulse for $M_{tip} = 0.95$

the shock is seen to get stronger with the increase in tip Mach number. Further, the radius of curvature of the spiral also becomes sharper as the M_{tip} increases, indicating a tighter shock spiral.

Figures 10 & 11 show the acoustic pressure pulse predicted by the FW-H solver, SIMULIA PowerACOUSTICS®. The predictions show reasonably good agreement with experimental data (Ref. 37) in both cases, especially in the higher tip Mach number case where a strong shock delocalization is known to occur. There is a slight under-prediction in the $M_{tip} = 0.85$ case and the cause behind this is currently under investigation.

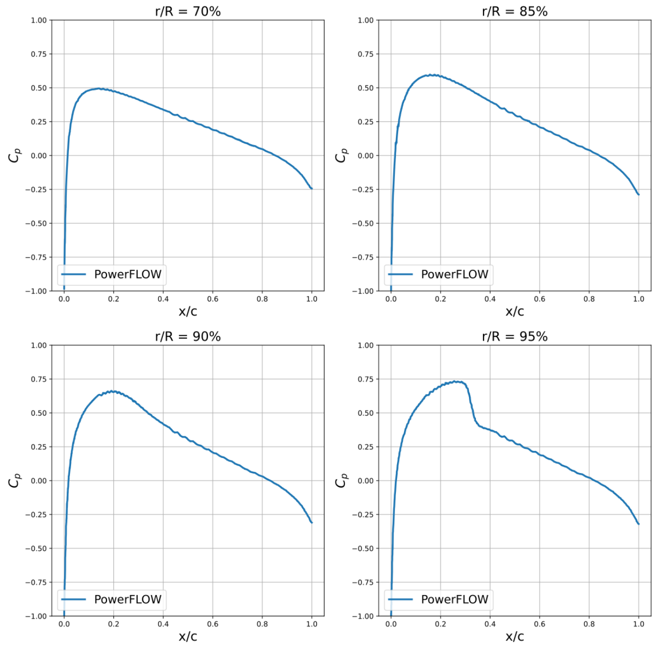

Figure 6. Surface Pressure distribution at different spanwise locations for $M_{tip} = 0.85$

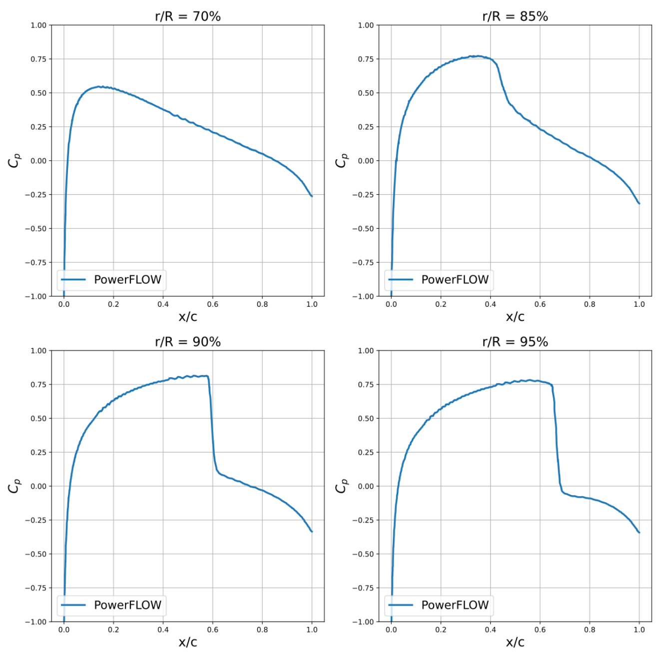

Figure 7. Surface Pressure distribution at different spanwise locations for $M_{tip} = 0.95$

CONCLUSIONS

The current study employed a high-fidelity framework to predict high-speed impulsive noise in transonic helicopter rotors. The solver comprised of the LB/VLES solver, SIMULIA PowerFLOW®, coupled with the time-domain FW-H solver, SIMULIA PowerACOUSTICS®. A transonic Lattice Boltzmann approach, suitable for high-speed flows, was used to model the flow and a permeable FW-H algorithm was used to model the acoustics. The benchmark UH-1H transonic ro-

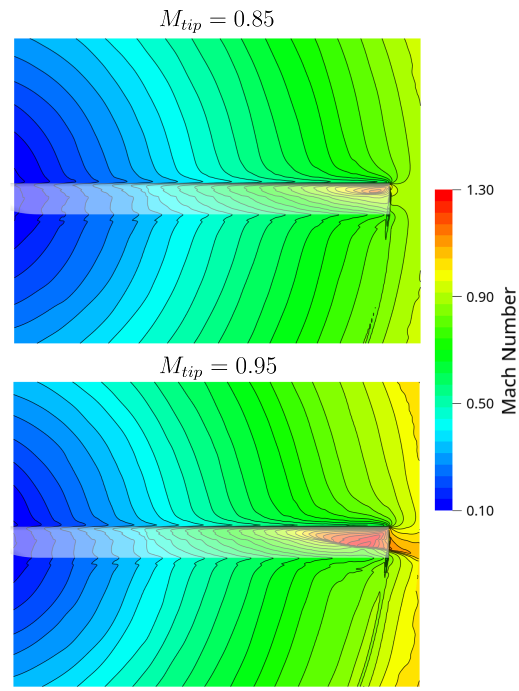

Figure 8. Mach number contour at different tip Mach numbers, demonstrating the shock delocalization phenomena.

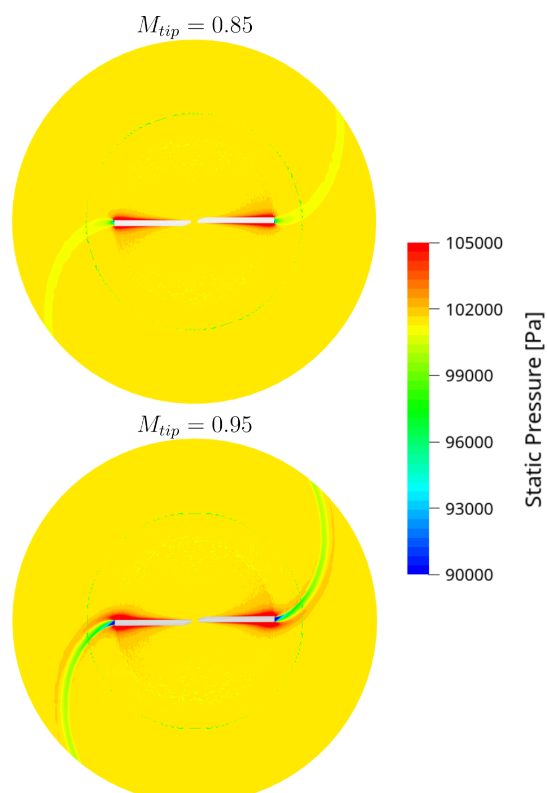

Figure 9. Static Pressure Contours at different tip Mach numbers.

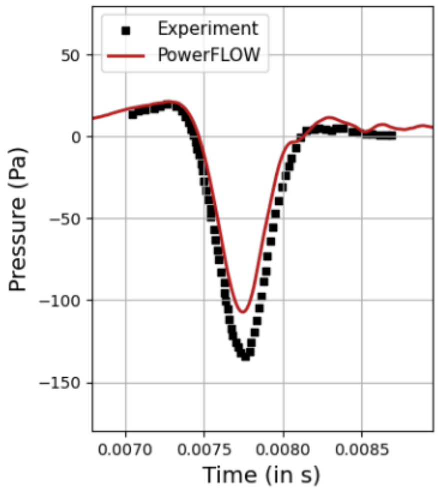

Figure 10. Acoustic Pressure at $M_{tip} = 0.85$

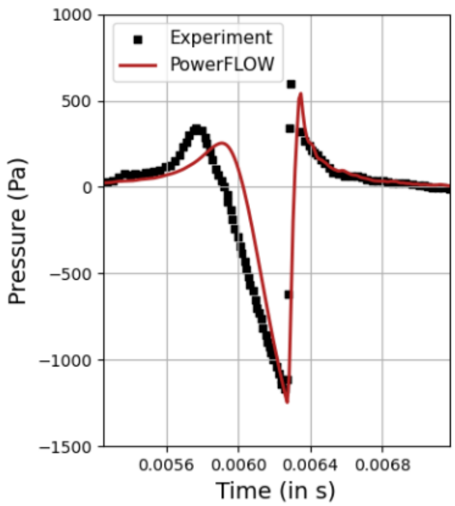

Figure 11. Acoustic Pressure at $M_{tip} = 0.95$

tor was used for validation. A grid resolution study was conducted to assess sensitivity in both aerodynamic and acoustic predictions. Simulations were performed at two tip Mach numbers: $M_{tip} = 0.85$ and $M_{tip} = 0.95$. The solver successfully captured localized shock formation at the lower Mach number and delocalized shocks at the higher Mach number. Acoustic predictions showed very good agreement with experimental data at both conditions. Overall, the computational framework demonstrated strong capability in accurately capturing transonic rotor flow and its associated noise.

Author contact:
Naina Pisharoti (naina.pisharoti@3ds.com)
Gianluca Romani (gianluca.romani@3ds.com)
Damiano Casalino (damiano.casalino@3ds.com)

REFERENCES

1. P. Di Francescantonio. A new boundary integral formulation for the prediction of sound radiation. *Journal of Sound and Vibration*, 202(4):491–509, 1997.
2. S. Ianniello. Quadrupole noise predictions through the ffowcs williams-hawkings equation. *AIAA Journal*, 37(9):1048–1054, September 1999.
3. Kenneth S Brentner and Feridoun Farassat. Modeling aerodynamically generated sound of helicopter rotors. *Progress in aerospace sciences*, 39(2-3):83–120, 2003.
4. S. Loiodice. Modelling noise from rotating sources in subsonic and supersonic regimes. *PhD Thesis, Cranfield University*, 2008.
5. Jinbin Fu and Luigi Vigevano. Aeroacoustic modeling of helicopter transonic rotor noise. *Aerospace Science and Technology*, 122:107430, 2022.
6. D. Casalino. An advanced time approach for acoustic analogy predictions. *Journal of Sound and Vibration*, 261(4):583–612, 2003.
7. M. Kessler and S. Wagner. Source-time dominant aeroacoustics. *Computers & Fluids*, 33:791–800, 2004.
8. N. Kroll, R. Radespiel, and C. Rossow. Structured grid solvers i - accurate and efficient flow solvers for 3d applications on structured meshes. *AGARD-R-807, Seiten 4.1-4.59, 1995*, 1995.
9. James D Baeder, Judith M Gallman, and Yung H Yu. A computational study of the aeroacoustics of rotors in hover. *Journal of the American Helicopter Society*, 42(1):39–53, 1997.
10. A. D'Alascio, P. Renzoni, and S. Ianniello. The eros aerodynamic analysis tool: an application towards the prediction of helicopter rotor noise in hover. *Aerotecnica Missili e Spazio*, 1999.
11. H. Chen, C. M. Teixeira, and K. Molvig. Realization of Fluid Boundary Conditions via Discrete Boltzmann Dynamics. *International Journal of Modern Physics C*, **9**(8):1281–1292, (1998),.
12. H. Chen, S. Kandasamy, S.Ã. Orszag, S. Succi, and V. Yakhot. Extended boltzmann kinetic equation for turbulent flows. *Science*, 301(5633):633–636, 2003.
13. H. Chen, S. Orszag, I. Staroselsky, and S. Succi. Expanded analogy between boltzmann kinetic theory of fluid and turbulence. *Journal of Fluid Mechanics*, 519:301–314, November 2004.
14. D. Casalino, A. F.P̃. Ribeiro, E. Fares, and S. Nölting. Lattice-boltzmann aeroacoustic analysis of the lagoon landing gear configuration. *AIAA Journal*, 52(6):1232–1248, 2014.
15. E. Fares, D. Casalino, and M. Khorrami. Evaluation of airframe noise reduction concepts via simulations using a lattice boltzmann approach. *AIAA Paper 2015-2988*, 2015.
16. E. Fares, B. Duda, A.F.P. Ribeiro, and B. König. Scale-resolving simulations using a lattice boltzmann-based approach. *CEAS Aeronautical Journal*, 9:721, 733, 2018.
17. Damiano Casalino, Edoardo Grande, Gianluca Romani, Daniele Ragni, and Francesco Avallone. Definition of a benchmark for low reynolds number propeller aeroacoustics. *Aerospace Science and Technology*, 113:106707, 2021.

18. Damiano Casalino, Gianluca Romani, Lorenzo Maria Pii, and Riccardo Colombo. Flow confinement effects on suas rotor noise. *Aerospace Science and Technology*, 143:108756, 2023.

19. G. Romani and D. Casalino. Rotorcraft blade-vortex interaction noise prediction using the lattice-boltzmann method. *Aerospace Science and Technology*, 800:147–157, 2019.

20. Gianluca Romani and Damiano Casalino. Powerflow simulations of helicopters in blade-vortex interaction conditions. In *Vertical Flight Society's 75th Annual Forum and Technology Display: The Future of Vertical Flight*, pages 49–60, 2019.

21. Damiano Casalino, Andreas Hazir, and Adrien Mann. Turbofan broadband noise prediction using the lattice boltzmann method. *AIAA Journal*, 56(2):609–628, 2018.

22. D. Cerizza, D. Casalino, and I. Gonzalez-Martino. An extension of the acoustics evaluation of the nasa sdt turbofan with lattice-boltzmann methods. *AIAA Paper 2022-2886*, 2022.

23. L. Rego, F. Avallone, D. Ragni, and D. Casalino. Jet-installation noise and near-field characteristics of jet-surface interaction. *Journal of Fluid Mechanics*, 895:A2, 2020.

24. Wende Li, Junye Wang, Pradeep Gopalakrishnan, Yanbing Li, Raoyang Zhang, and Hudong Chen. Hybrid lattice boltzmann approach for simulation of high-speed flows. *AIAA Journal*, 61(12):5548–5557, 2023.

25. Hudong Chen, Raoyang Zhang, and Pradeep Gopalakrishnan. Filtered lattice boltzmann collision formulation enforcing isotropy and galilean invariance. *Physica Scripta*, 95(3):034003, 2020.

26. Raoyang Zhang, Hongli Fan, and Hudong Chen. A lattice boltzmann approach for solving scalar transport equations. *Philosophical Transactions of the Royal Society A: Mathematical, Physical and Engineering Sciences*, 369(1944):2264–2273, 2011.

27. Pradeep Gopalakrishnan, Hudong Chen, Raoyang Zhang, Avinash Jammalamadaka, and Yanbing Li. Lattice boltzmann solver enforcing total energy conservation, July 5 2022. US Patent 11,379,636.

28. Raoyang Zhang, Chenghai Sun, Yanbing Li, Rajani Satti, Richard Shock, James Hoch, and Hudong Chen. Lattice boltzmann approach for local reference frames. *Communications in Computational Physics*, 9(5):1193–1205, 2011.

29. V. Yakhot and S.Ã. Orszag. Renormalization group analysis of turbulence. i. basic theory. *Journal of Scientific Computing*, 1(1):3–51, 1986.

30. V. Yakhot, S.Ã. Orszag, S. Thangam, T.B̃. Gatski, and C.G̃. Speziale. Development of turbulence models for shear flows by a double expansion technique. *Physics of Fluids A*, 4(7):1510–1520, 1992.

31. R. B. Kotapati, R. Shock, and H. Chen. Lattice-Boltzmann Simulations of Flows Over Backward-Facing Inclined Steps. *International Journal of Modern Physics C*, **25**(01):1340021, (2014), publisher=World Scientific.

32. B.Ẽ. Launder and D.B̃. Spalding. The numerical computation of turbulent flows. *Computer Methods in Applied Mechanics and Engineering*, 3:269–269, 1974.

33. C.M̃. Teixeira. Incorporating turbulence models into the lattice-boltzmann method. *International Journal of Modern Physics C*, 9:1159–1175, 1998.

34. John E Ffowcs Williams and David L Hawkings. Sound generation by turbulence and surfaces in arbitrary motion. *Philosophical Transactions of the Royal Society of London. Series A, Mathematical and Physical Sciences*, 264(1151):321–342, 1969.

35. Damiano Casalino. An advanced time approach for acoustic analogy predictions. *Journal of Sound and Vibration*, 261(4):583–612, 2003.

36. Fereidoun Farassat. Derivation of formulations 1 and 1a of farassat. Technical report, 2007.

37. T. W. Purcell. Cfd and transonic helicopter sound. *Associazione Industrie Aerospaziali and Associazione Italiana di Aeronautica ed Astronautica*, 1988.